ACS APPLIED MATERIALS & INTERFACES

www.acsami.org

Research Article

Impact of Surface Modification on the Lithium, Sodium, and Potassium Intercalation Efficiency and Capacity of Few-Layer Graphene Electrodes

A. Nijamudheen, Dipobrato Sarbapalli, Jingshu Hui, Joaquín Rodríguez-López,* and Jose L. Mendoza-Cortes*

Cite This: *ACS Appl. Mater. Interfaces* 2020, 12, 19393−19401

Read Online

ACCESS | Metrics & More | Article Recommendations | Supporting Information

ABSTRACT: In a conventional lithium-ion battery (LIB), graphite forms the negative electrode or anode. Although Na is considered one of the most attractive alternatives to Li, achieving reversible Na intercalation within graphitic materials under ambient conditions remains a challenge. More efficient carbonaceous anode materials are desired for developing advanced LIBs and *beyond Li-ion* battery technologies. We hypothesized that two-dimensional materials with distinct surface electronic properties create conditions for ion insertion into few-layer graphene (FLG) anodes. This is because modification of the electrode/electrolyte interface potentially modifies the energetics and mechanisms of ion intercalation in the thin bulk of FLG. Through first-principles calculations; we show that the electronic, structural, and thermodynamic properties of FLG anodes can be fine-tuned by a covalent heteroatom substitution at the uppermost layer of the FLG electrode, or by interfacing FLG with a single-side fluorinated graphene or a Janus-type hydrofluorographene monolayer. When suitably interfaced with the 2D surface modifier, FLG exhibits favorable thermodynamics for the Li^+, Na^+, and K^+ intercalation. Remarkably, the reversible binding of Na within carbon layers becomes thermodynamically allowed, and a large storage capacity can be achieved for the Na intercalated modified FLG anodes. The origin of charge-transfer promoted electronic tunability of modified FLGs is rationalized by various theoretical methods.

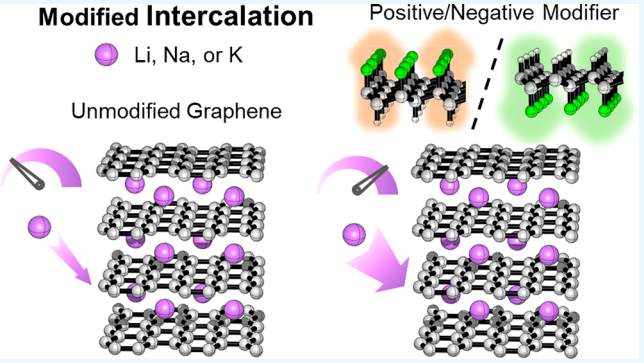

KEYWORDS: *beyond Li-ion battery, Na-ion battery, DFT, fluorinated graphene, energy storage, few-layers graphene*

1. INTRODUCTION

Portable electronic devices rely on lithium ion battery (LIB) technology for storing electrical energy. Affordable and more efficient technologies should be developed to fulfill the mounting demands for Li-ion batteries in portable and wearable electronics, smart grids, electric vehicles, and other renewable energy storage devices.[1−8] The cost, efficiency, cyclability, and the safety of a LIB depend critically on its three major components; the electrodes, the electrolyte, and the *in situ* formed solid−electrolyte interphase (SEI). Over the past four decades, several studies have focused on improving the overall LIB performance by investigating the roles played by each of its major components and by modifying or replacing the materials used.[3−9] The commercially available LIB typically employs a graphite based negative electrode (anode) because the latter is inexpensive, thermodynamically stable, and abundant in nature and affords favorable reversible intercalation of Li ions.[10,11] Following the success of graphite, researchers have been trying to improve the LIB performance by using alternative carbonaceous anode materials. One promising strategy in this direction is to replace the graphite anode by its two-dimensional analogue, few-layer graphene (FLG) or graphene composites.[12−14] Studies have shown improved specific capacity, smaller ion diffusion path, and faster Li-ion transport for FLG electrodes.[15−20] Controlled electrochemical experiments have revealed some of the unique intercalation and deintercalation pathways in FLG electrodes.[21,22] An understanding of the thermodynamics and kinetics of reversible Li-ion intercalation in graphene layers can accelerate the experimental investigations to improve the stability, cyclability, storage capacity, and safety of the traditional LIB.

Received: December 21, 2019
Accepted: February 28, 2020
Published: February 28, 2020

https://dx.doi.org/10.1021/acsami.9b23105
ACS Appl. Mater. Interfaces 2020, 12, 19393−19401

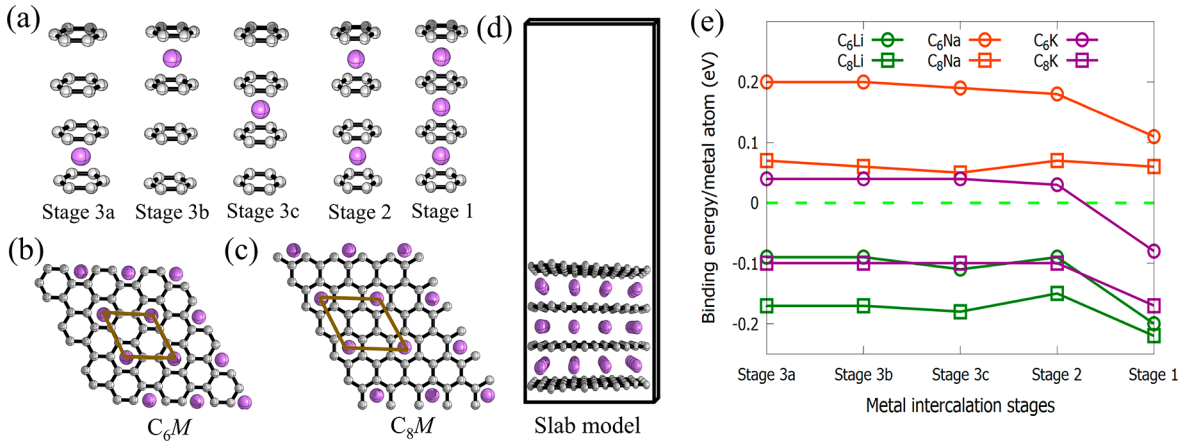

Figure 1. Models used to study the metal intercalation chemistry in a four-layer graphene (4LG) anode. (a) Optimized geometries of Li intercalated 4LG (Li−4LG) at different stages. (b, c) Top views of C_6Li and C_8Li models, where only the top graphene layer and the metal atoms are shown for clarity. The unit cells are represented by solid brown lines. (d) Side view of the optimized geometry of Stage 1 of Li−4LG with a C_6Li concentration. Similar models are used to study the Na and K intercalation mechanisms and corresponding electronic properties. (e) Variation in calculated binding energy per metal atom (eV) for different stages of metal (M = Li, Na, and K) intercalation.

The demand for LIB has been increasing worldwide, and if the consumption rates continue to grow, it is estimated that most of the mineable Li-ion resources could be used up in the next 6−7 decades.[23−25] Na and K ions are abundant in nature and are less expensive compared to Li.[26−29] Incorporating Na and K ions in existing battery technologies may be feasible because Li, Na, and K ions share similar chemical properties. Sodium- and potassium-ion batteries (SIB and KIB, respectively) have other advantages, such as the presence of a large negative anode potential and superior cathode performances. However, there are potential barriers that limit the fabrication and the practical use of SIB and KIB technologies.[26−28] Notably, SIB suffers from a poor storage capacity and unfavorable ion intercalation thermodynamics and kinetics. We posit that modification of surface structures and their processes could improve the performance toward Na and K. Indeed, a recent study from our groups showed that this is the case for K.[9] However, a deeper inspection into the potential effects that a modified interface could bring for intercalation on FLG is desirable. The present study focuses on addressing the issues of metal intercalation/deintercalation efficiency and the thermodynamic stability of anodes for LIB, SIB, and KIB through a theoretical investigation.

One less-explored design strategy to improve the performance of metal (Li, Na, and K) ion batteries is tuning the electronic and thermodynamic properties of the electrodes by forming interfaces with surface modifying layers. We speculated that carbonaceous two-dimensional materials with distinct electronic properties can act as suitable surface modifiers for FLG electrodes. To test our hypothesis, we first modeled a Janus-type hydrofluorinated graphene 2D-HC_2F as the surface modifier (SM).[30] 2D-HC_2F is selected because it is a unique, highly polarized system with distinct positive and negative surfaces. This enabled us to use the same material to investigate the effects due to the negative and positive surface modifications of FLG layers, *i.e.*, interfacing with the negatively and positively polarized surfaces of SM with graphene layers. Although 2D-HC_2F has not been experimentally realized yet, its molecular analogue was recently synthesized and showed excellent tunable optoelectronic properties.[31−34] Quantum mechanical investigations have elucidated that synthesis of 2D-HC_2F may be feasible, and the material can tune the properties of graphene layers.[30,35] Several researchers have synthesized partially and fully fluorinated graphene layers and have studied their electronic, mechanical, and chemical properties.[36−41] Therefore, after establishing the potential of surface modifications using 2D-HC_2F, we turned our attention to the applications of experimentally realizable and stable, single-side fluorinated graphene as the SM. Remarkably, single-side fluorinated graphene also showed significant tunability for FLG properties.

We used first-principles calculations to understand the details of reversible metal (M = Li, Na, and K) intercalation mechanisms in FLG. Many unique *M* concentrations and intercalation configurations are studied. The results indicate that SM layers can provide significant stabilization energy for the metal intercalated systems through charge-transfer mechanisms. By applying the surface modification strategy, even Na-ion intercalation within the FLG can be made thermodynamically favorable. Apart from increasing the intercalation energies, the surface modification also imparts enhanced storage capacity to the FLG anode. We unravel the factors that lead to the stabilization of SM-tuned anode structures from a systematic study of geometrical and electronic properties.

2. COMPUTATIONAL METHODS

Geometry optimizations and other electronic structure calculations are performed using the plane-wave density functional theory (DFT) methods within the generalized gradient approximation of Perdew, Burke, and Ernzerhof (GGA-PBE).[42] We used the projector-augmented wave (PAW) pseudopotentials to represent the core electrons and ion−electron interactions.[43] A plane-wave cutoff of 500 eV, energy convergence criterion of 10^{-4} eV, and a force convergence criterion of 0.02 eV were utilized for the geometry optimizations. All calculations included spin-polarization effects. For the electronic structure analysis, we employed tighter plane-wave cutoff, energy convergence, and force convergence criteria of 700 eV, 10^{-5} eV, and 0.001 eV, respectively. Similarly, we used Γ-point centered 6 × 6 × 1 and 10 × 10 × 1 *k*-point meshes for geometry optimizations and electronic structure analyses, respectively. We find that the calculation setups could produce reasonably accurate structures and electronic properties for the systems studied here. The long-range effects and the van der Waal's interactions are included in the DFT calculations by

https://dx.doi.org/10.1021/acsami.9b23105
ACS Appl. Mater. Interfaces 2020, 12, 19393−19401

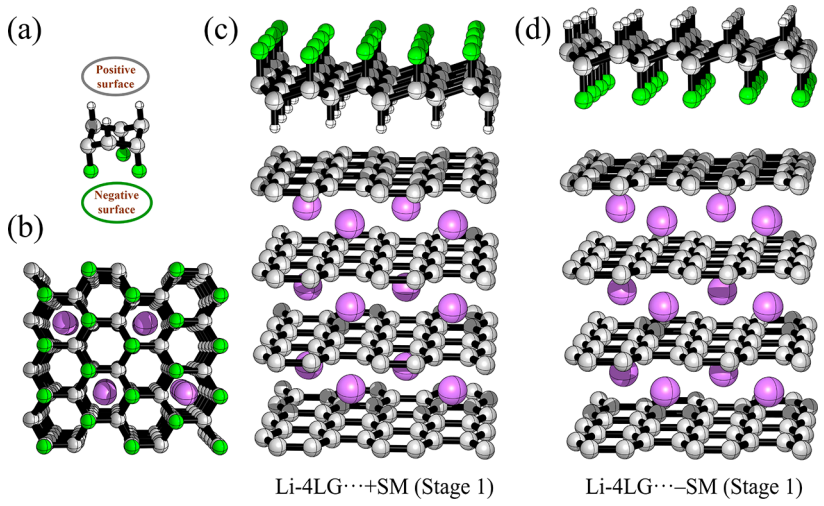

Figure 2. (a) Representative unit of the surface modifier (SM) hydrofluorinated graphene (HFG or 2D-HC_2F). Both the negative (F-layer) and positive (H-layer) surfaces of the modifying monolayer are highlighted. (b) Top view of a positive SM modified *M*−4LG (Li−4LG···+SM). (c, d) Side views of *M*−4LG interfaced with positive and negative SM, respectively.

the Grimme's empirical dispersion correction scheme, leading to the computationally efficient DFT-D3 technique.[44] The DFT-D3 computations are implemented by the plane-wave DFT code Vienna *Ab Initio* Simulation Package (VASP).[45,46] For the calculations of two-dimensional (2D) and slab-model systems, interlayer interactions are avoided by incorporating an additional vacuum space of ∼12−15 Å in the simulation cell.

Binding energy per metal (M = Li, Na, and K) atom for *M* intercalated pristine (4LG) and surface modifier interfaced four-layer graphene (SM-4LG) were calculated by eqs 1 and 2, respectively.

$$\frac{\Delta E_{M-4LG}}{n} = \frac{E_{M-4LG} - n[E_M + E_{coh}] - E_{4LG}}{n} \quad (1)$$

$$\frac{\Delta E_{M-SM-4LG}}{n} = \frac{E_{M-SM-4LG} - n[E_M + E_{coh}] - E_{SM-4LG}}{n} \quad (2)$$

where $\frac{\Delta E_{M-4LG}}{n}$ and $\frac{\Delta E_{M-SM-4LG}}{n}$ represent the binding energy per *M* atom for the *M* intercalated in 4LG and SM−4LG, respectively. E_{M-4LG}, E_{4LG}, and E_M are the energies of metal intercalated, free 4LG, and a single metal atom, respectively. $E_{M-SM-4LG}$ and E_{SM-4LG} denote the energies of metal intercalated and free SM−4GL, respectively. Finally, n is the number of intercalated metal atoms and E_{coh} is the experimental cohesive energy of a metal atom in its stable, bulk metallic crystalline form. The current models of metal intercalated systems replicates the state of the anode when the battery is fully charged. Previous computational studies have demonstrated that the methodologies adopted here are suitable to model the thermochemical and dynamical properties of metal-ion intercalations in battery materials.[47,48]

3. RESULTS AND DISCUSSIONS

We now discuss the structural and electronic properties of *M* intercalated FLG and SM−FLG in distinct configurations and concentrations.

3.1. Metal Intercalation in Four-Layer Graphene (4LG) Anode. Recent experiments using precisely size-controlled FLG models have demonstrated interesting staging mechanisms for the metalation processes.[21] Building on these ideas, we model three distinct stages within a four-layer graphene (4LG) anode. Stages 3, 2, and 1 represent the metalation of one, two, and three interlayers, respectively, of the 4LG (Figure 1a). Stages 3a and 3b represent the same structure in the absence of a SM but show different levels of stability in its presence. Experimentally feasible maximum Li and K intercalation in graphite under ambient conditions furnishes the stoichiometry of C_6Li and C_8K, respectively, for Stage 1.[49,50] However, both C_6Na and C_8Na stoichiometries are thermodynamically unstable for any of configurations studied. To evaluate the metalation capacity trends and staging mechanisms, we have calculated thermodynamic stabilities for different stages of C_6M and C_8M configurations, where M = Li, Na, and K (Figure 1b,c). We note that the stoichiometries C_6M and C_8M are possible only for intercalation in bulk graphite or for adsorption over monolayer graphene. In a 4LG, the concentration of intercalated *M* in these configurations will be smaller because there are only 3 interlayers for a total of 4 graphene layers in our models. To be consistent with the terminology used in the literature, here we use the terms C_6M and C_8M to represent the configuration with respect to a graphene monolayer or bulk graphite (Figure 1b,c) than the actual concentration of *M* with respect to 4LG.

Our calculations show that lithiation in 4LG is thermodynamically stable for all configurations studied with the maximum stability found for Stage 1 (Figure 1e). At Stage 1, C_6Li and C_8Li structures have similar binding energy per atom (BE/atom) of −0.20 and −0.22 eV, respectively. These stabilization energies are comparable to the values obtained from previous calorimetric measurements (∼−0.15 eV)[51] and computational benchmark studies (−0.17 and −0.20 eV) for C_6Li.[48,50] The calculated average interlayer distance of 3.62 Å for C_6Li at Stage 1 is comparable with the experimentally measured value of 3.70 Å.[52,53] Sodiation is thermodynamically unstable for any stage. Nevertheless, the C_8Na configuration is more favorable than the C_6Na structures (by 0.05 eV/atom for Stage 1). Calculated interlayer distances for C_6Na and C_8Na configurations of Stage 1 are 4.39 and 4.45 Å, respectively. It is well-known that Na intercalation of graphite is thermodynamically unfavorable.[47,54] Similar to the sodiation, potassiation is favored for the C_8K structures than C_6K (by 0.09 eV/atom for Stage 1). All stages of C_8K structures are stable with the maximum stability achieved for experimentally found C_8K Stage 1 structures (BE/atom = −0.17 eV). Our calculations and previous experiments show the same graphene interlayer distance of 5.35 Å for Stage 1 of C_8K.[55,56] The above results

https://dx.doi.org/10.1021/acsami.9b23105
ACS Appl. Mater. Interfaces 2020, 12, 19393−19401

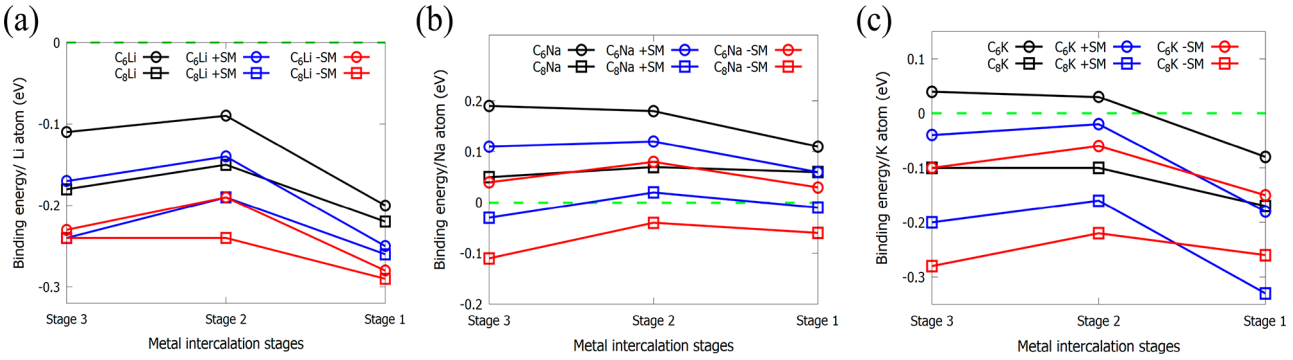

Figure 3. Variations in BE per *M* atom (eV) for *M*−4LG systems interfaced with positive (+SM) or negative (−SM) surface modifiers. M = Li, Na, and K in panels a−c, respectively. For Stage 3, only the energies corresponding to the most stable configurations are presented for brevity.

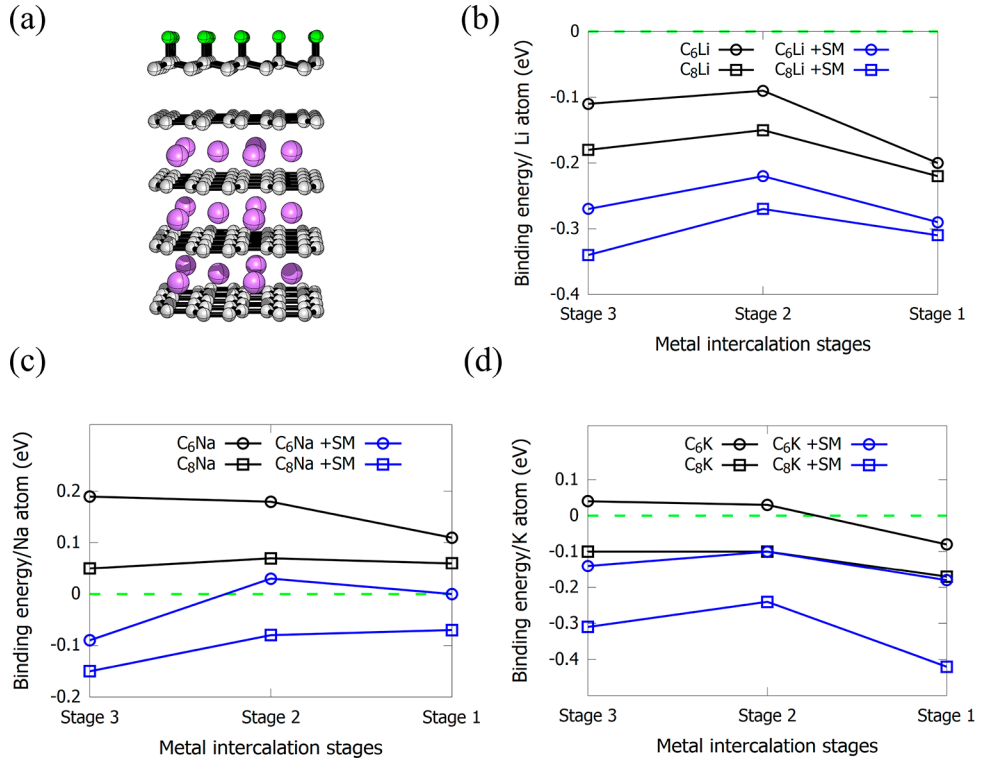

Figure 4. Using single-side fluorinated graphene, 2D-C_2F, as the SM: (a) optimized geometry for the Stage 1 of Li-SM−4LG and (b−d) plots of calculated BE per *M* atom (eV) for *M*−SM−4LG (SM = 2D-C_2F). For Stage 3, only the energies corresponding to the most stable configurations are presented.

further corroborate the suitability of our models and calculations setup to study the structural, electronic, and thermodynamic properties of alkali metal intercalated FLG systems.

3.2. Metal Intercalation of 4LG Modified with Surface Modifier (SM). On the basis of the charge density and polarity, F-face and H-face of SM hydrofluorinated graphene (HFG or 2D-HC_2F) are named as negative and positive surfaces, respectively (Figure 2a). We find that, regardless of a positive or negative surface modification, the presence of a SM layer increases the thermodynamic preferences for Li intercalation within a FLG electrode (Figure 3a). For small Li concentration, the presence of a negative SM increases the BE/atom for Li intercalation substantially. We have studied the effects of SM on all three different configurations of Stage 3 (Figure 1) in both C_6M- and C_8M-type systems. The negative SM increases BE/Li atom at Stage 3b by 0.14−0.15 eV compared to pristine 4LG (Tables S1 and S2). The electron-rich F-layer increases the charge localization and polarizability of immediate graphene layer and the Li intercalation. Weak long-range effects due to the negative SM for Stages 3a and 3c are reflected in their enhanced thermodynamic stabilities. This also indicates that the effects due to the surface modification are distance dependent and the overall effects could be decreased as we increase the number of graphene layers. In Stage 1, a combination of the short- and long-range effects furnishes the total stability gain of 0.08 eV per Li atom. Positive SM modification is expected to decrease the BE/atom for *M* intercalation because such modification will decrease the charge localization of immediate graphene layers below SM. However, long-range effects resulting from positive SM modifications lead to stability gain, albeit in smaller magnitudes. Surface modification by the positive surface

https://dx.doi.org/10.1021/acsami.9b23105
ACS Appl. Mater. Interfaces 2020, 12, 19393−19401

increases the BE/atom by 0.05−0.08 eV for different Li intercalation stages.

Next, we looked at the effects of SM on the Na intercalated structures. Remarkably for all stages with a C_8Na configuration, Na intercalation is thermodynamically feasible when interfaced with a negative SM (Figure 3b). As expected, the BE/atom is largest for Stage 3b; the value increased by ∼0.17 eV due to SM (the structures of Stage 3 with SM in configurations a−c are presented in Figure S1). For Stage 1 of C_8Na, calculations predict a BE/atom of −0.06 eV for the negative SM interfaced 4LG (C_8Na−SM) compared to 0.06 for pristine 4LG (C_8Na). Although the overall Na intercalation energy is small, the results indicate that the surface modifications using 2D layers is a promising approach to achieve favorable Na intercalation in FLG anodes. Positive SM modifications also improve the energetics for Na intercalation processes. However, the resulting BE/atom is still around 0 eV, indicating that electronic structure tuning by positive SM is not large enough for practical Na intercalation in these systems. Compared to the Li or Na intercalation, the BE/atom for K intercalation is affected largely by SM modifications (Figure 3c). Negative SM increases the BE per K atom for Stage 3b and Stage 1 by up to 0.18 and 0.09 eV, respectively. Even the positive SM increases the thermodynamics stability for Stage 1 of C_8K configuration substantially. All of these results further suggest two-dimensional SM modifications as a promising strategy to improve the capacity and thermodynamics for *M* intercalated FLG electrodes.

Here, we have discussed the structures and energetics for heterojunctions designed by parallel stacking (Figure 2b) of 4LG with SM either via a positive or negative surface (Figure 2c,d). Other possible arrangements (slipped-parallel stack) and corresponding energetics are also calculated, and results presented in Figure S2 and Table S3, respectively. Thus, we predict that the stacking configurations do not affect the thermodynamic preferences for the metal intercalation/deintercalation with 4LG. The stability of the interface is another critical parameter. We predict nonsignificant energy changes due to the binding of SM with the 4LG in a parallel or a slipped-parallel stacking fashion. *Ab initio* molecular dynamics calculations carried out at ∼300 K on selected systems revealed that the SM modified structures are stable during the simulation time.

Using Single-Side Fluorinated Graphene as the SM to Tune M-4LG Properties. The Janus-type SM discussed here is yet to be synthesized in a stable form. Therefore, we explored the possibility of an experimentally realizable (though typically <50% fluorination is found in experiments)[57−59] and thermodynamically stable single-side fluorinated graphene (2D-C_2F) as the SM. We modeled several unique configurations and stages of *M*−4LG in the presence of 2D-C_2F SM. Calculations demonstrated that 2D-C_2F could improve the thermodynamics of *M*−4LG (Li, Na, and K) in a fashion similar to that predicted when 2D-HC_2F is used as the SM (Figure 4, Table S4). The SM affected the intercalation for all different *M* concentrations studied. The binding energies changed even more in the presence of 2D-C_2F than with 2D-HC_2F. Evidently, the SM increased *M* intercalation energies in all different stages for any *M*. For *M* = Li, C_6M configurations are more stable than C_8M configurations. For *M* = Na or K, C_8M configurations are thermodynamically more stable. Even Na interaction in 4LG is thermodynamically favored in the presence of SM. Experimentally, the mild radical fluorination of the topmost layer of FLG electrode can generate the SM-tuned electrode.[36−40,57,58] Therefore, we expect that the predictions made here could be directly verified from experiments.

In order to find the maximum storage capacity of pristine and modified 4LG anodes, we studied the intercalation energies when there are five layers of *M* binding with four layers of C. We termed this structure as Stage 0 to distinguish from the 3 stages we discussed earlier. The structures of Stage 0 and corresponding intercalation energies are presented in Figure 5 and Table 1, respectively. We computed the maximum theoretical specific capacity (C_W) for Na intercalation within Na−SM−4LG (SM = 2D-C_2F) by applying eq 3.

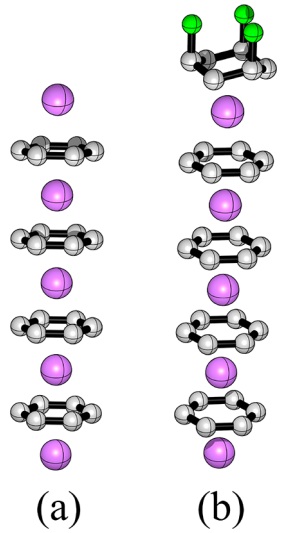

Figure 5. Optimized geometries for Stage 0 of (a) Li−4LG and (b) Li−SM−4LG.

$$C_W = \frac{n \times Z \times F \times 1000}{W(\mathrm{Na-SM-4LG})} \quad (3)$$

In eq 3 *n* is the number of Na atoms intercalated, *Z* is the valence number (=1 for Na), *F* is the Faraday constant (26.810 Ah/mol), and *W*(Na−SM−4LG) is the total atomic mass of Stage 0 of Na−SM−4LG. Calculations predict a maximum specific capacity of 252 mAh g^{-1} for Na intercalation within a SM interfaced 4LG anode. The predicted theoretical specific capacity is significantly larger than the small storage capacity of <35 mAh g^{-1} found experimentally for the pristine graphite anode.[20,60] Although a recent combined experimental and theoretical investigation[61] has demonstrated that multilayers of Li intercalation within a bilayer graphene are possible, we have not considered these possibilities in our calculations.

Distortion-Interaction Model Analysis to Reveal the Effects of SM on the Energetics of M Intercalation. We applied a distortion-interaction model to partition and analyze different energy components that contribute to the overall stability of a metal intercalated 4LG either in the presence or absence of a SM monolayer. According to the distortion-interaction model, the total BE/atom is broken into three energy terms (eq 4).

$$\mathrm{BE/atom} = E_{\mathrm{dist}} + E_{\mathrm{coh}} + E_{\mathrm{int}} \quad (4)$$

https://dx.doi.org/10.1021/acsami.9b23105
ACS Appl. Mater. Interfaces 2020, 12, 19393−19401

Table 1. Calculated Binding Energies (BEs) for Stage 0 of *M*−4LG and *M*−SM−4LG (SM = 2D-C_2F)

	BE per metal atom (eV)					
	C_6M-type models			C_8M-type models		
system	with SM, 2D-C_2F (no SM = pristine 4LG)			with SM, 2D-C_2F (no SM = pristine 4LG)		
intercalated metal	Li	Na	K	Li	Na	K
Stage 0	−0.35 (0.05)	−0.17 (0.12)	−0.38 (−0.09)	−0.33 (0.10)	−0.20 (0.18)	−0.42 (−0.15)

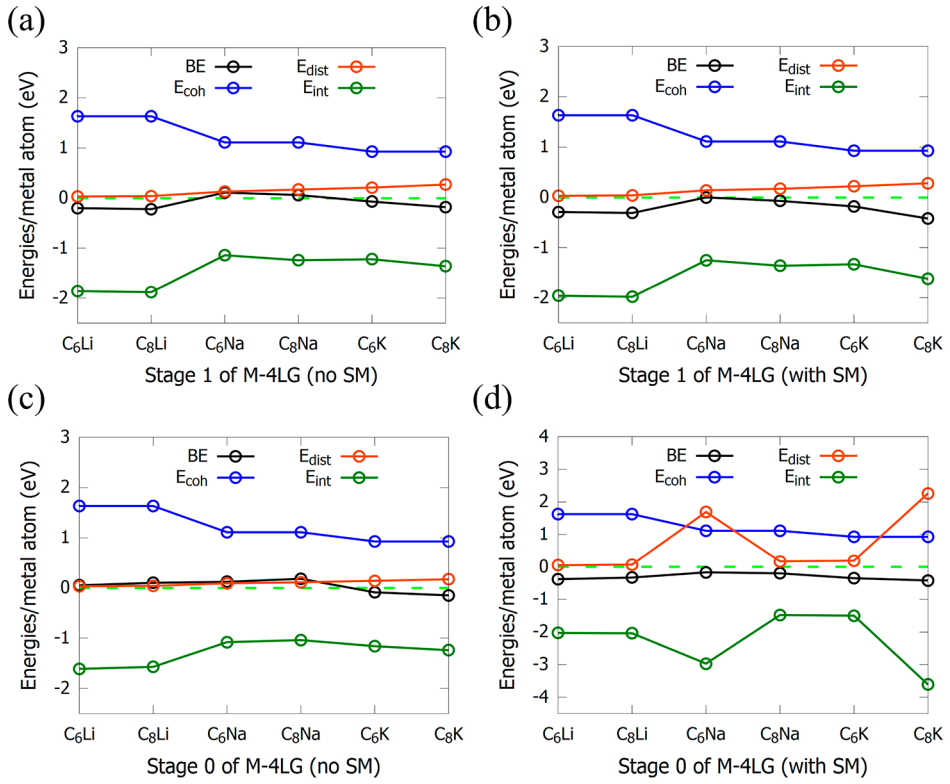

Figure 6. Energy decomposition analyses of Stage 1 (a, b) and Stage 0 (c, d) structures of *M*−4LG and SM−*M*−4LG based on a distortion-interaction model.

where E_{dist} is the energy required for distorting and activating 4LG from its equilibrium structure to the geometry of the *M* intercaled state, *M*−4LG. E_{coh} is the experimental cohesive energy of *M* with respect to its stable bulk metallic form. In other words, E_{coh} is the energy required to evaporate the bulk metal to its isolated atoms. E_{int} is the interaction energy between the *M* and the strained (activated) 4LG. While BE/atom and E_{coh} are experimentally measurable quantities, both the terms E_{dist} and E_{int} can only be computed from theoretical calculations. We have plotted all of these energy terms for Stage 1 and Stage 0 of *M*−4LG systems (Figure 6). As we go down the group from Li to K, the magnitude of E_{coh} shows a gradual decrease (Tables S5 and S6). The strain energy increases from Li to K because E_{dist} depends critically on the size of the metal atom. Evidently, the magnitude of E_{int} is independent of the size of *M* and follows the same trends found for BE/atom. Therefore, we conclude that the interaction energy between *M* and strained 4LG determines the overall stability of the metal intercalated systems. The smallest E_{int} found for Na intercalated 4LG systems contribute to the instability of Na intercalated systems. A recent report by Liu et al. has also utilized the energy decomposition analysis presented here to explain the intrinsic instability of Na intercalated bulk graphite anodes.[47] Next, we studied the effects of SM on different energy components. The presence of a SM leads to negligible or no changes in the E_{dist}, but substantially increases the E_{int}. The increase in E_{int} is almost independent of the nature of the *M*. However, a larger change is present for Stage 0 compared to Stage 1 because in the former systems, the SM has a short-range interaction possible with the metalated immediate layers. This eventually makes Stage 0 thermodynamically stable even for Na intercalated systems.

Density of States (DOS) Calculations. The electronic properties of the *M*−4LG anodes both in the presence and the absence of a SM (here 2D-C_2F) layer are investigated by computing and analyzing their projected density of states (pDOS). The DOS calculations indicated that irrespective of the presence or absence of a SM, the *M* intercalated systems show metallic behavior. When going from Stage 3 to Stage 0, contributions from the Li subshells near the Fermi level gradually increased (Figure 7). The valence band edge (VBE) states of the SM-tuned systems are largely affected by the occupied F subshells. The interaction of F 2p states with the C 2p and *M* valence s orbitals could be responsible for the increased intercalation energies found for SM-tuned anodes.

A comparison of the pDOS of C_6Li and 2D-C_2F−C_6Li (Figure S3) points that significant charge-transfer-type

https://dx.doi.org/10.1021/acsami.9b23105
ACS Appl. Mater. Interfaces 2020, 12, 19393−19401

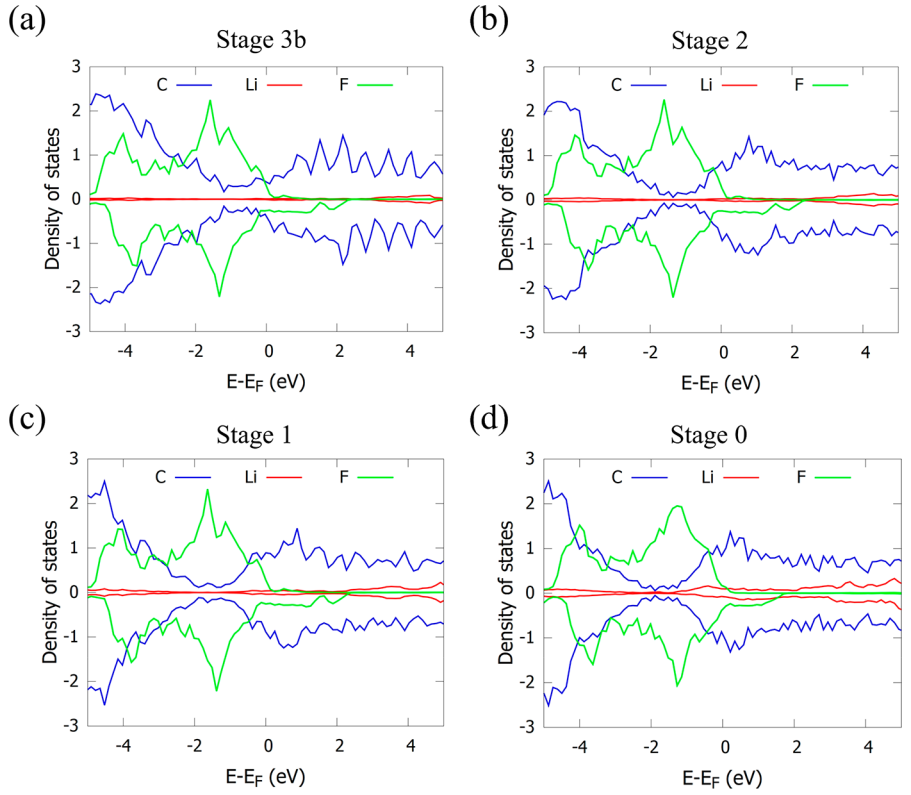

Figure 7. Calculated density of states of Li intercalated SM−4LG (SM = 2D-C_2F) systems with a C_6M-type configuration at (a) Stage 3b, (b) Stage 2, (c) Stage 1, and (d) Stage 0.

interactions between the occupied 2p orbitals of F and C are possible. The Na intercalated systems showed negligible Na 2p orbital participation near the band edges than the Li or K intercalated systems. This explains the small binding affinity found for the Na with FLG anodes. Although the C_2F layer does not directly change the DOSs of *M* atoms, the matching of energy ranges and hybridization of 2p F with respect to the C 2p orbitals lead to favorable interaction of the F and C subshells near the Fermi level and provides superior *M* intercalation properties. The average atomic charge of C in the top layer of *M*−4LG changed significantly in the presence of 2D-C_2F.[62] For *M* = Li, Na, and K; the average charges of top-layer C atoms are −0.10, −0.08, and −0.07, respectively, in Stage 1 of *M*−4LG; and −0.06, −0.05, and −0.05, respectively, in 2D-C_2F modified *M*−4LG. Although the charge transfer between SM and C is evident, the presence of SM does not directly change the *M* charges. Average atomic charges on Li, Na, and K are 0.85, 0.82, and 0.74, respectively, in *M*−4LG and 0.84, 0.82, and 0.76 in 2D-C_2F modified *M*−4LG. Therefore, both DOS calculations and charge analysis indicate that the charge transfer between SM and C atoms will contribute to increased interaction energy (E_{int}) between the graphene and the intercalated *M*.

4. CONCLUSIONS

First-principles calculations revealed the energetics for metal (*M* = Li, Na, and K) intercalation within a 4LG anode. Li or K intercalation within the 4LG leads to stable structures with varying binding energies depending on the *M* concentration, whereas the Na intercalation leads to energetically unstable materials. When *M* = Li, the C_6M-type structures are favored over C_8M-type structures, whereas an opposite trend is found for *M* = Na or K. Further, our calculations indicate that the electronic properties of the 4LG can be tuned by interfacing the anode with a surface modifier (SM) layer. When a Janus-type 2D monolayer (2D-C_2HF) is used as SM, the *M* intercalation energies increased by long-range charge-transfer interactions between SM and 4LG. Notably, when the negatively polarized and F-rich surface of the SM is interfaced with 4LG, even Na intercalation within C-layers becomes thermodynamically favorable.

After establishing that a theoretically predicted 2D-C_2HF SM can favor the *M* intercalation within 4LG, we investigated the applications of an experimentally realizable single-side fluorinated graphene monolayer (2D-C_2F) as the SM. Calculations predicted that apart from increasing the metal intercalation energies in several stages, 2D-C_2F can also enhance the metal storage capacity of the anode. Although SM considered here (2D-C_2HF and 2D-C_2F) are semiconductors, *M* intercalated SM−4LG demonstrates metallic properties. The charge-transfer interactions leading to the superior intercalation properties of SM−FLG anodes are studied through the analysis of pDOS in them. Practically, it is possible to synthesize the 2D-C_2F−interfaced-FLG by the fluorination of the top C-layer of a pristine FLG. We believe that our predictions could be tested experimentally through the fabrication of top-layer fluorinated FLG anodes.

■ ASSOCIATED CONTENT

Supporting Information

The Supporting Information is available free of charge at https://pubs.acs.org/doi/10.1021/acsami.9b23105.

Interlayer stacking distances (Å) in metal intercalated 4LG during different stages, thermodynamic parameters

https://dx.doi.org/10.1021/acsami.9b23105
ACS Appl. Mater. Interfaces 2020, 12, 19393−19401

for *M* intercalation within a 4LG either in the presence or absence of different SM, different stacking arrangements for SM with 4LG, and corresponding energies, table of energy terms obtained from energy decomposition analysis, DOSs calculated for selected M-intercalated systems (PDF)

AUTHOR INFORMATION

Corresponding Authors

Joaquín Rodríguez-López − *Department of Chemistry, University of Illinois at Urbana−Champaign, Urbana, Illinois 61801, United States;* orcid.org/0000-0003-4346-4668; Email: joaquinr@illinois.edu

Jose L. Mendoza-Cortes − *Department of Chemical & Biomedical Engineering, Florida A&M University—Florida State University (FAMU-FSU) College of Engineering, Tallahassee, Florida 32310, United States; Department of Scientific Computing, Materials Science and Engineering, High Performance Materials Institute, Condensed Matter Theory—National High Magnetic Field Laboratory (NHMFL) and Department of Physics, College of Arts and Science, Florida State University, Tallahassee, Florida 32310, United States;* orcid.org/0000-0001-5184-1406; Email: mendoza@eng.famu.fsu.edu

Authors

A. Nijamudheen − *Department of Chemical & Biomedical Engineering, Florida A&M University—Florida State University (FAMU-FSU) College of Engineering, Tallahassee, Florida 32310, United States; Department of Scientific Computing, Materials Science and Engineering, High Performance Materials Institute, Condensed Matter Theory—National High Magnetic Field Laboratory (NHMFL), Florida State University, Tallahassee, Florida 32310, United States;* orcid.org/0000-0001-9191-1851

Dipobrato Sarbapalli − *Department of Chemistry and Department of Materials Science and Engineering, University of Illinois at Urbana−Champaign, Urbana, Illinois 61801, United States*

Jingshu Hui − *Department of Chemistry, University of Illinois at Urbana−Champaign, Urbana, Illinois 61801, United States;* orcid.org/0000-0002-6987-4414

Complete contact information is available at: https://pubs.acs.org/10.1021/acsami.9b23105

Notes

The authors declare no competing financial interest.

ACKNOWLEDGMENTS

This material is based upon work supported by the National Science Foundation under Grant No. NSF DMR 1905803. A.N. and J.L.M-C. thank the High-Performance Computer (HPC) facility at the Research Computing Center (RCC) in Florida State University (FSU) for providing computational resources and support. A.N. and J.L.M-C. gratefully acknowledge the support from the High-Performance Material Institute (HPMI) facilities at FSU.

REFERENCES

(1) Tarascon, J.-M.; Armand, M. Issues and Challenges Facing Rechargeable Lithium Batteries. *Nature* **2001**, *414*, 359−367.

(2) Armand, M.; Tarascon, J.-M. Building Better Batteries. *Nature* **2008**, *451*, 652−657.

(3) Goodenough, J. B.; Kim, Y. Challenges for Rechargeable Li Batteries. *Chem. Mater.* **2010**, *22*, 587−603.

(4) Dunn, B.; Kamath, H.; Tarascon, J.-M. Electrical Energy Storage for the Grid: A Battery of Choices. *Science (Washington, DC, U. S.)* **2011**, *334*, 928−935.

(5) Thackeray, M. M.; Wolverton, C.; Isaacs, E. D. Electrical Energy Storage for Transportation: Approaching the Limits of, and Going beyond, Lithium-Ion Batteries. *Energy Environ. Sci.* **2012**, *5*, 7854−7863.

(6) Goodenough, J. B.; Park, K.-S. The Li-Ion Rechargeable Battery: A Perspective. *J. Am. Chem. Soc.* **2013**, *135*, 1167−1176.

(7) Nitta, N.; Wu, F.; Lee, J. T.; Yushin, G. Li-Ion Battery Materials: Present and Future. *Mater. Today* **2015**, *18*, 252−264.

(8) Choi, J. W.; Aurbach, D. Promise and Reality of Post-Lithium-Ion Batteries with High Energy Densities. *Nat. Rev. Mater.* **2016**, *1*, 16013.

(9) Hui, J.; Schorr, N. B.; Pakhira, S.; Qu, Z.; Mendoza-Cortes, J. L.; Rodríguez-López, J. Achieving Fast and Efficient K^+ Intercalation on Ultrathin Graphene Electrodes Modified by a Li^+ Based Solid-Electrolyte Interphase. *J. Am. Chem. Soc.* **2018**, *140*, 13599−13603.

(10) Sawai, K.; Iwakoshi, Y.; Ohzuku, T. Carbon Materials for Lithium-Ion (Shuttlecock) Cells. *Solid State Ionics* **1994**, *69*, 273−283.

(11) Brandt, K. Historical Development of Secondary Lithium Batteries. *Solid State Ionics* **1994**, *69*, 173−183.

(12) Brownson, D. A. C.; Kampouris, D. K.; Banks, C. E. An Overview of Graphene in Energy Production and Storage Applications. *J. Power Sources* **2011**, *196*, 4873−4885.

(13) Murugan, A. V.; Muraliganth, T.; Manthiram, A. Rapid, Facile Microwave-Solvothermal Synthesis of Graphene Nanosheets and Their Polyaniline Nanocomposites for Energy Strorage. *Chem. Mater.* **2009**, *21*, 5004−5006.

(14) Kumar, A.; Reddy, A. L. M.; Mukherjee, A.; Dubey, M.; Zhan, X.; Singh, N.; Ci, L.; Billups, W. E.; Nagurny, J.; Mital, G.; et al. Direct Synthesis of Lithium-Intercalated Graphene for Electrochemical Energy Storage Application. *ACS Nano* **2011**, *5*, 4345−4349.

(15) Wang, C.; Li, D.; Too, C. O.; Wallace, G. G. Electrochemical Properties of Graphene Paper Electrodes Used in Lithium Batteries. *Chem. Mater.* **2009**, *21*, 2604−2606.

(16) Zhou, G.; Wang, D.-W.; Li, F.; Zhang, L.; Li, N.; Wu, Z.-S.; Wen, L.; Lu, G. Q. M.; Cheng, H.-M. Graphene-Wrapped Fe_3O_4 Anode Material with Improved Reversible Capacity and Cyclic Stability for Lithium Ion Batteries. *Chem. Mater.* **2010**, *22*, 5306−5313.

(17) Lian, P.; Zhu, X.; Liang, S.; Li, Z.; Yang, W.; Wang, H. Large Reversible Capacity of High Quality Graphene Sheets as an Anode Material for Lithium-Ion Batteries. *Electrochim. Acta* **2010**, *55*, 3909−3914.

(18) Wu, Z.-S.; Ren, W.; Xu, L.; Li, F.; Cheng, H.-M. Doped Graphene Sheets As Anode Materials with Superhigh Rate and Large Capacity for Lithium Ion Batteries. *ACS Nano* **2011**, *5*, 5463−5471.

(19) Xu, J.; Mahmood, J.; Dou, Y.; Dou, S.; Li, F.; Dai, L.; Baek, J.-B. 2D Frameworks of C_2N and C_3N as New Anode Materials for Lithium-Ion Batteries. *Adv. Mater.* **2017**, *29*, 1702007.

(20) Kühne, M.; Paolucci, F.; Popovic, J.; Ostrovsky, P. M.; Maier, J.; Smet, J. H. Ultrafast Lithium Diffusion in Bilayer Graphene. *Nat. Nanotechnol.* **2017**, *12*, 895−900.

(21) Hui, J.; Burgess, M.; Zhang, J.; Rodríguez-López, J. Layer Number Dependence of Li^+ Intercalation on Few-Layer Graphene and Electrochemical Imaging of Its Solid−Electrolyte Interphase Evolution. *ACS Nano* **2016**, *10*, 4248−4257.

(22) Petnikota, S.; Rotte, N. K.; Srikanth, V. V. S. S.; Kota, B. S. R.; Reddy, M. V.; Loh, K. P.; Chowdari, B. V. R. Electrochemical Studies of Few-Layered Graphene as an Anode Material for Li Ion Batteries. *J. Solid State Electrochem.* **2014**, *18*, 941−949.

(23) Hwang, J.-Y.; Myung, S.-T.; Sun, Y.-K. Sodium-Ion Batteries: Present and Future. *Chem. Soc. Rev.* **2017**, *46*, 3529−3614.

(24) Pan, H.; Hu, Y. S.; Chen, L. Room-Temperature Stationary Sodium-Ion Batteries for Large-Scale Electric Energy Storage. *Energy Environ. Sci.* **2013**, *6*, 2338−2360.
(25) Olivetti, E. A.; Ceder, G.; Gaustad, G. G.; Fu, X. Lithium-Ion Battery Supply Chain Considerations: Analysis of Potential Bottlenecks in Critical. *Metals. Joule* **2017**, *1*, 229−243.
(26) Slater, M. D.; Kim, D.; Lee, E.; Johnson, C. S. Sodium-Ion Batteries. *Adv. Funct. Mater.* **2013**, *23*, 947−958.
(27) Wu, X.; Leonard, D. P.; Ji, X. Emerging Non-Aqueous Potassium-Ion Batteries: Challenges and Opportunities. *Chem. Mater.* **2017**, *29*, 5031−5042.
(28) Luo, W.; Wan, J.; Ozdemir, B.; Bao, W.; Chen, Y.; Dai, J.; Lin, H.; Xu, Y.; Gu, F.; Barone, V.; Hu, L. Potassium Ion Batteries with Graphitic Materials. *Nano Lett.* **2015**, *15*, 7671−7677.
(29) Yabuuchi, N.; Kubota, K.; Dahbi, M.; Komaba, S. Research Development on Sodium-Ion Batteries. *Chem. Rev.* **2014**, *114*, 11636−11682.
(30) Singh, R.; Bester, G. Hydrofluorinated Graphene: Two-Dimensional Analog of Polyvinylidene Fluoride. *Phys. Rev. B: Condens. Matter Mater. Phys.* **2011**, *84*, 155427.
(31) Keddie, N. S.; Slawin, A. M. Z.; Lebl, T.; Philp, D.; O'Hagan, D. All-Cis 1,2,3,4,5,6-Hexafluorocyclohexane Is a Facially Polarized Cyclohexane. *Nat. Chem.* **2015**, *7*, 483−488.
(32) Ziegler, B. E.; Lecours, M.; Marta, R. A.; Featherstone, J.; Fillion, E.; Hopkins, W. S.; Steinmetz, V.; Keddie, N. S.; O'Hagan, D.; McMahon, T. B. Janus Face Aspect of All-Cis 1,2,3,4,5,6-Hexafluorocyclohexane Dictates Remarkable Anion and Cation Interactions In the Gas Phase. *J. Am. Chem. Soc.* **2016**, *138*, 7460−7463.
(33) Pratik, S. M.; Nijamudheen, A.; Datta, A. Janus All-Cis-1,2,3,4,5,6-Hexafluorocyclohexane: A Molecular Motif for Aggregation-Induced Enhanced Polarization. *ChemPhysChem* **2016**, *17*, 2373−2381.
(34) Wiesenfeldt, M. P.; Nairoukh, Z.; Li, W.; Glorius, F. Hydrogenation of Fluoroarenes: Direct Access to All- Cis -(Multi)-Fluorinated Cycloalkanes. *Science (Washington, DC, U. S.)* **2017**, *357*, 908−912.
(35) Pratik, S. M.; Nijamudheen, A.; Datta, A. Design of van Der Waals Two-Dimensional Heterostructures from Facially Polarized Janus All-Cis 1,2,3,4,5,6-Hexafluorocyclohexane ($C_6H_6F_6$). *J. Phys. Chem. C* **2017**, *121*, 1752−1762.
(36) Nair, R. R.; Ren, W.; Jalil, R.; Riaz, I.; Kravets, V. G.; Britnell, L.; Blake, P.; Schedin, F.; Mayorov, A. S.; Yuan, S.; Katsnelson, M. I.; Cheng, H.-M.; Strupinski, W.; Bulusheva, L. G.; Okotrub, A. V.; Grigorieva, I. V.; Grigorenko, A. N.; Novoselov, K. S.; Geim, A. K. Fluorographene: A Two-Dimensional Counterpart of Teflon. *Small* **2010**, *6*, 2877−2884.
(37) Jeon, K.-J.; Lee, Z.; Pollak, E.; Moreschini, L.; Bostwick, A.; Park, C.-M.; Mendelsberg, R.; Radmilovic, V.; Kostecki, R.; Richardson, T. J.; Rotenberg, E. Fluorographene: A Wide Bandgap Semiconductor with Ultraviolet Luminescence. *ACS Nano* **2011**, *5*, 1042−1046.
(38) Withers, F.; Bointon, T. H.; Dubois, M.; Russo, S.; Craciun, M. F. Nanopatterning of Fluorinated Graphene by Electron Beam Irradiation. *Nano Lett.* **2011**, *11*, 3912−3916.
(39) Nair, R. R.; Sepioni, M.; Tsai, I.-L.; Lehtinen, O.; Keinonen, J.; Krasheninnikov, A. V.; Thomson, T.; Geim, A. K.; Grigorieva, I. V. Spin-Half Paramagnetism in Graphene Induced by Point Defects. *Nat. Phys.* **2012**, *8*, 199−202.
(40) Şahin, H.; Topsakal, M.; Ciraci, S. Structures of Fluorinated Graphene and Their Signatures. *Phys. Rev. B: Condens. Matter Mater. Phys.* **2011**, *83*, 115432.
(41) Nijamudheen, A.; Datta, A. Pattern Formation Due to Fluorination on Graphene Fragments: Structures, Hopping Behavior, and Magnetic Properties. *J. Phys. Chem. A* **2013**, *117*, 8506−8511.
(42) Perdew, J. P.; Burke, K.; Ernzerhof, M. Generalized Gradient Approximation Made Simple. *Phys. Rev. Lett.* **1996**, *77*, 3865−3868.
(43) Blochl, P. E. Projector Augmented-Wave Method. *Phys. Rev. B: Condens. Matter Mater. Phys.* **1994**, *50*, 17953−17979.
(44) Grimme, S.; Antony, J.; Ehrlich, S.; Krieg, H. A Consistent and Accurate Ab Initio Parametrization of Density Functional Dispersion Correction (DFT-D) for the 94 Elements H-Pu. *J. Chem. Phys.* **2010**, *132*, 154104.
(45) Kresse, G.; Furthmüller, J. Efficient Iterative Schemes for Ab Initio Total-Energy Calculations Using a Plane-Wave Basis Set. *Phys. Rev. B: Condens. Matter Mater. Phys.* **1996**, *54*, 11169−11186.
(46) Kresse, G.; Hafner, J. Ab Initio Molecular Dynamics for Liquid Metals. *Phys. Rev. B: Condens. Matter Mater. Phys.* **1993**, *47*, 558−561.
(47) Liu, Y.; Merinov, B. V.; Goddard, W. A. Origin of Low Sodium Capacity in Graphite and Generally Weak Substrate Binding of Na and Mg among Alkali and Alkaline Earth Metals. *Proc. Natl. Acad. Sci. U. S. A.* **2016**, *113*, 3735−3739.
(48) Hazrati, E.; de Wijs, G. A.; Brocks, G. Li Intercalation in Graphite: A van Der Waals Density-Functional Study. *Phys. Rev. B: Condens. Matter Mater. Phys.* **2014**, *90*, 155448.
(49) Jian, Z.; Luo, W.; Ji, X. Carbon Electrodes for K-Ion Batteries. *J. Am. Chem. Soc.* **2015**, *137*, 11566−11569.
(50) Wang, Z.; Selbach, S. M.; Grande, T. Van Der Waals Density Functional Study of the Energetics of Alkali Metal Intercalation in Graphite. *RSC Adv.* **2014**, *4*, 3973−3983.
(51) Avdeev, V. V.; Savchenkova, A. P.; Monyakina, L. A.; Nikol'skaya, I. V.; Khvostov, A. V. Intercalation Reactions and Carbide Formation in Graphite-Lithium System. *J. Phys. Chem. Solids* **1996**, *57*, 947−949.
(52) Billaud, D.; Henry, F. X.; Lelaurain, M.; Willmann, P. Revisited Structures of Dense and Dilute Stage II Lithium-Graphite Intercalation Compounds. *J. Phys. Chem. Solids* **1996**, *57*, 775−781.
(53) Takami, N.; Satoh, A.; Hara, M.; Ohsaki, T. Structural and Kinetic Characterization of Lithium Intercalation into Carbon Anodes for Secondary Lithium Batteries. *J. Electrochem. Soc.* **1995**, *142*, 371−379.
(54) Moriwake, H.; Kuwabara, A.; Fisher, C. A. J.; Ikuhara, Y. Why Is Sodium-Intercalated Graphite Unstable? *RSC Adv.* **2017**, *7*, 36550−36554.
(55) Zhao, J.; Zou, X.; Zhu, Y.; Xu, Y.; Wang, C. Electrochemical Intercalation of Potassium into Graphite. *Adv. Funct. Mater.* **2016**, *26*, 8103−8110.
(56) Dresselhaus, M. S.; Dresselhaus, G. Intercalation Compounds of Graphite. *Adv. Phys.* **2002**, *51*, 1−186.
(57) Wang, B.; Wang, J.; Zhu, J. Fluorination of Graphene: A Spectroscopic and Microscopic Study. *ACS Nano* **2014**, *8*, 1862−1870.
(58) Son, J.; Kwon, J.; Kim, S.; Lv, Y.; Yu, J.; Lee, J.-Y.; Ryu, H.; Watanabe, K.; Taniguchi, T.; Garrido-Menacho, R.; Mason, N.; Ertekin, E.; Huang, P. Y.; Lee, G.-H.; van der Zande, A. M. Atomically Precise Graphene Etch Stops for Three Dimensional Integrated Systems from Two Dimensional Material Heterostructures. *Nat. Commun.* **2018**, *9*, 3988.
(59) Robinson, J. T.; Burgess, J. S.; Junkermeier, C. E.; Badescu, S. C.; Reinecke, T. L.; Perkins, F. K.; Zalalutdniov, M. K.; Baldwin, J. W.; Culbertson, J. C.; Sheehan, P. E.; Snow, E. S. Properties of Fluorinated Graphene Films. *Nano Lett.* **2010**, *10*, 3001−3005.
(60) Stevens, D. A.; Dahn, J. R. The Mechanisms of Lithium and Sodium Insertion in Carbon Materials. *J. Electrochem. Soc.* **2001**, *148*, A803.
(61) Kühne, M.; Börrnert, F.; Fecher, S.; Ghorbani-Asl, M.; Biskupek, J.; Samuelis, D.; Krasheninnikov, A. V.; Kaiser, U.; Smet, J. H. Reversible Superdense Ordering of Lithium between Two Graphene Sheets. *Nature* **2018**, *564*, 234−239.
(62) Tang, W.; Sanville, E.; Henkelman, G. A Grid-Based Bader Analysis Algorithm without Lattice Bias. *J. Phys.: Condens. Matter* **2009**, *21*, 084204.

https://dx.doi.org/10.1021/acsami.9b23105
ACS Appl. Mater. Interfaces 2020, 12, 19393−19401